Journal Homepage: - www.journalijar.com

INTERNATIONAL JOURNAL OF ADVANCED RESEARCH (IJAR)

Article DOI: 10.21474/IJAR01/16935
DOI URL: http://dx.doi.org/10.21474/IJAR01/16935

RESEARCH ARTICLE

SURFACE ROUGHNESS CHANGE IN THE HEAT TREATMENT OF Ti-6Al-4V EXTRA LOW INTERSTITIAL ALLOY

Muslim Efendi Harahap, Nandang Suhendra, Masmui, Bambang Triwibowo, Suryadi, Mutmainah and Fitri Kurniawati
National Agency for Research and Innovation (BRIN), Republic of Indonesia (KST Prof. B.J. Habibie, Jl. Raya Puspiptek, Tangerang Selatan Banten, Indonesia 15314).

Manuscript Info

Manuscript History
Received: 20 March 2023
Final Accepted: 22 April 2023
Published: May 2023

Key words:-
Heat Treatment, Fractal Dimension, Surface Roughness, Ti-6Al-4V, ELI Alloy

Abstract

The heat treatment improves the casting result's structure and changes the alloy's microstructure. The fractal dimension of the Ti-6Al-4V Extra Low Interstitial (ELI) alloy changes with the alteration of surface roughness under various heat treatment conditions. This study used three primary raw materials: first-grade Titanium, pure aluminum, and pure vanadium. The SEM images of the sample were translated into topographic data. The Fractal Dimension (FD) calculation results that the surface's topography appearing throughout the heat treatment temperatures and has fractal features. The Heat Treatment (HT) process shows a close relationship between heat treatment temperature and fractal dimension. Surface roughness after heat treatment at 1050^{o}C is smoother than at 850^{o}C and 950^{o}C.

Copy Right, IJAR, 2023. All rights reserved.

Introduction:-

Titanium alloys are widely used for various applications, including aerospace, chemical, and biomedical industries. This alloy is widely applied because it has good mechanical properties and high corrosion resistance. The biocompatibility properties of Ti6Al4V ELI allow it to be used for biomedical applications as implant materials, especially the Ti-6Al-4V Extra Low Alloy Interstitial, otherwise known as Ti-6AL-4V ELI, with 6% aluminum content and 4% vanadium which is a popular alloy titanium for application biomedical implants. Compared with Conventional Ti-6Al-4V, this ELI class has lower impurities, especially an oxygen maximum of 0.13% **[1]** Therefore, the Ti-6AL-4V alloy has better tenacity and higher crack toughness. Some examples of medical implants that use Ti-6Al-4V ELI include artificial knee and hip joint prosthesis implants, therapeutic orthopedics, and dental implants **[2]** . The price of titanium alloy and the production costs are high; therefore, net-shape technology or near-net-shape has received much attention **[3]** . This technology can produce a product close to the desired final technology, and the cost of complex-shaped implants will be more efficient. However, this technology's disadvantages are necessary for the heat treatment process to reduce casting defects, improve microstructure, and improve the alloy's mechanical properties **[4]** .

Many techniques, like heat treatment and alloying, have been employed recently to enhance the overall characteristics of 6Al-4V ELI alloys **[2]** ,**[5]** . Current treatment, mainly done by dissolving at a temperature of 100^{o}C above transus-beta, promotes microstructure transformation and improves an alloy's properties in its solid state. This temperature is at the lowest equilibrium point with the material in the 100% beta phase condition.

Corresponding Author:- Muslim Efendi Harahap
Address:- National Agency for Research and Innovation (BRIN) Republic of Indonesia KST Prof. B.J. Habibie, Jl. Raya Puspiptek, Tangerang Selatan, Banten, Indonesia 15314.

Cooling can be fast and slow. The martensite reaction will decompose the phase at a rapid cooling rate and form the Widmanstätten structure **[6]** ,**[7]**

Excessive statistical characteristics representing surface lay elements, roughness, waviness, and form can describe surface topography **[8]** . Unfortunately, many of them heavily depend on the measurement methods, such as instrument resolution, scan durations, and sampling. Fractal geometry has been offered to describe engineering surfaces **[8]** . Fractals are imaginary, self-similar geometrical objects that, regardless of the magnification scale, appear to be identical. These items exhibit the fractal dimension D **[9]** .

Fractal Dimension

A brief review of fractal dimension background. Presents literature on surface morphology calculation, analysis, and fractal–heat treatment **[9] ,[10] [11]** . Two kinds of image processing methods were used on the SEM images before calculating fractal dimensions, 8-bit/pixel (black and white photos) and 64-bit/pixel (RGB) **[12]** . The predicted fractal dimensions produced by the current method for the three different heat-treating temperatures.

The study of surface roughness or heterogeneity can be divided into three categories or trades, namely (A) surface defect at atomic and molecular levels, from 0.1 nm up, which can be detected by field electron microscopy, low energy electron diffraction conveys only gross information about hidden surface; (B) intermediate region extending from some 100 nm downwards, namely internal surface, porosimetry takes over; in this size level surface irregularity is described in term of pore-width distribution; (C) surface topography from around 100 nm upward which optical microscopy and electron micrographs (particle profiles) in term of Fourier coefficients, i.e., in term of roundness, elongation, thickness, etc. **[13]** . Those categories of surface roughness of materials are illustrated in **Figure 1 [13]** .

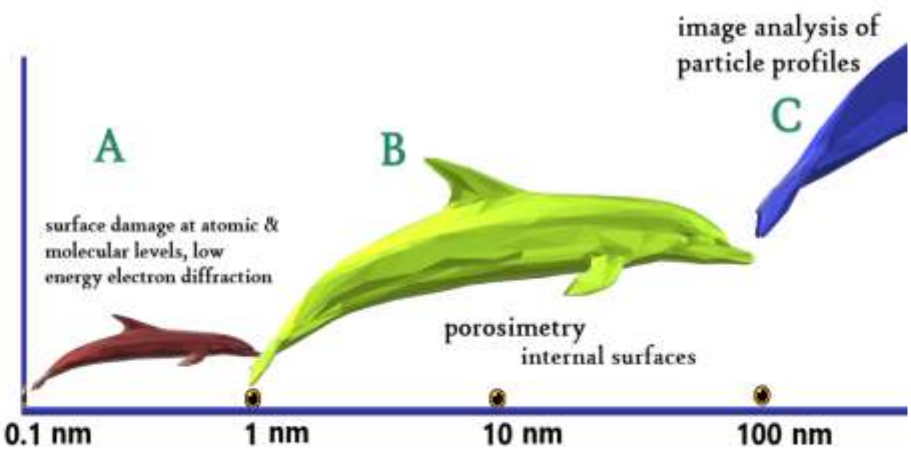

Figure 1:- Surface Roughness Scale-Size Categories.

The fractal dimension measurement D of surface roughness was implemented in the study of fractal surfaces **[13]** . Not all surface roughness is a fractal type **[13]** . Fractal dimension characteristics, categorized into A, B, or C, make them comparable **[13]** . Surface roughness parameters are discovered to be linked with fractal dimension **[14]** ,**[15]** , **[16]** ,**[17]** . It is connected to many material characteristics **[18]** and processes that produce surfaces **[19]** . The potential impact of each numerical method on the outcomes needs to be understood **[9]** . The notion of a box-count dimension is investigated by assessing the fractal dimension using cube counts. An initial cubic cell with an edge length of L equal to the scan length is iteratively divided into smaller cubes by the algorithm. The number of all cubes with at least one sample of a 3D topography is counted, or N(L). The process is continued until L reaches the image resolution or the distance between two neighboring models **[9]** , since:

$$N(L) \propto L^{-D} \quad (1)$$

The fractal dimension, known as the cube count fractal dimension D_{CC}, is determined by the slope of a log-log plot of N(L) vs. L. The surface height variance's root-mean-squared value, or S_q, is used to estimate the fractal dimension and is defined as **[9]** :

$$S_q = \sqrt{\frac{1}{N_x N_y}\sum_{i=0}^{Nx-1}\sum_{j=0}^{Ny-1}(z(i,j) - \langle z \rangle)^2} \quad (2)$$

Where z(i,j) represents the measured height in an image pixel (i,j); N_x and N_y denote the number of samples along rows and columns in the image—assuming that the scale of the surface roughness S_q measured over surfaces with various edge lengths L:

$$S_q \propto L^{3-D} \quad (3)$$

The fractal dimension D_{RMS} can be calculated from the slope of a least-square regression line fitted in a log-log plot of S_q vs. L [19] **[20]** .

Characterization and Surface Topography Analysis Methods

Three techniques for calculating a surface's fractal dimension are based on fractal analysis of the surface's contour (horizontal section), profile, and size (vertical section). As stated in **[21]** , the relationship between the values obtained for the fractal dimensions is as follows:

$$D_c = D_p = D - 1 \quad (1)$$

D is the surface contour's fractal dimension, and D_p is the profile's fractal dimension. Since actual surfaces do not have the same fractal dimension across all scales, the concept of multifractals is used. A multifractal is a group of structures having specific in a subset of parts and fractal dimensions in materials science. The idea of multifractals is employed since natural surfaces do not have the same fractal dimension across all sizes. In materials science, multifractals are employed since natural surfaces do not have the same fractal dimension across all sizes. Multifractals are defined by a spectrum D_q using the relation **[18]** :

$$D_c = D_p = D - 1 \quad (1)$$

A spectrum D_q characterizes multifractals with the relation **[22]** where ε is the size of a cell in a network encompassing the item of interest; p_i is the relative population, i.e., the likelihood that a point is in the i^{th} cell of size ε ; q is an exponent that can assume any value from – ∞ to + ∞; N is the number of cells; and, $\sum_{i=1}^{N} p_i^q$ is a generalized statistical sum providing information on the system's statistical features. Thus, for q → – ∞ cells with a small relative population p_i contribute the most to the total, and for q → + ∞, the cells with the highest significant number of points contribute the most. If D_q = constant, the set is an ordinary fractal; if the function D_q changes with q, the group is fractal **[22]** .

Materials and Method:-

This study used three primary raw materials: first-grade Titanium, pure aluminum, and pure vanadium. We calculate material balance to obtain the Ti-6Al-4V ELI alloy to meet the ASTM F 136 standard. Moreover, we weighed the raw materials as needed and melted them in a laboratory-scale single-arc melting furnace. The Ti Grade 1 raw material fed is 27 grams, while aluminum and vanadium total 3 grams. Meanwhile, the Ti6Al-4V ELI ingot obtained was 30 grams. In the smelting process, high-purity argon gas flows. After the entire raw material is melted, the metal melt is allowed to freeze in crucibles, and a button-shaped ingot is produced. The bars were tested with Optical Emission Spectroscopy (Oxford Instrument, Foundry Master Pro) to determine their chemical composition **[23]** .

Then, the ingots carried out a heat treatment with solution treatment, followed by a cooling process **[23]** fast in a water medium (quenching). The dissolution practice is given for 1 hour with argon gas. The treatment used variable temperatures, including 850^{o}C, 950^{o}C, and 1050^o C. After that, the aging process was carried out for 4 hours at a temperature of 500^{o}C. Both dissolution and aging treatments were carried out in an argon gas environment.

The Ti-6Al-4V ELI sample was then observed with an optical microscope (Olympus Microscope equipped with an E4500 type camera) with some magnification to observe its microstructure. Before following the microstructure, prepare the sample metallographically by grinding, polishing, and etching. The etching solution used is a solution of Dix-Keller reagent, which consists of a mixture of nitric acid solution (HNO_3), hydrochloric acid (HCl), and hydrofluoric acid (HF).

In particular research, grayscale pictures generated by SEM must be translated into topographic data before being utilized for further computations. The Fractal Dimension (FD) calculation results of the two approaches are very different **[9] .** As a result, it was required to pay close attention to the source of topographical data before fractal analysis **[9] .**

Previous research has discovered that the topography's microstructure appears throughout the heat treatment temperatures and has fractal features **[24]** . The FD can assess topographical complexity and investigate the impact of preparation circumstances on topographical quality **[25]** . Various approaches have been employed recently to compute the FD of different heat treatment temperatures properties **[4]** ,**[24]** .

Results and Discussion:-

The observations using an optical microscope for the as-cast Ti-6Al-4V ELI alloy before undergoing heat treatment are shown in **Figure 2** below. **Figure 2** shows that the as-cast sample has a dendritic structure characteristic of casting products. This dendritic structure will be visible if observed with higher magnification, as in **Figure 2(b).** While in general, alloys have a lamellar α and β phase structure and form webbing connected, or what is often known as a basket-weave structure. Observation of the microstructure with an optical microscope shows that the alloy has an α phase characterized by a light-colored area.

(a) (b)

Figure 2:- Optical Image of Ti-6Al-4V ELI Surface Before Undergoing Heat Treatment (a) 200X and 500X.

In contrast, the dark-colored area is the β phase. The α phase is formed at the prior β grain boundary, and this grain boundary limits the growth of the α grain. The same result was obtained by Oh et al. and Pinke et al. with the Ti-6Al-4V as-cast microstructure showing the Widmanstätten structure consisting of α phases and lamellar-shaped β **[26]** , **[27]** .

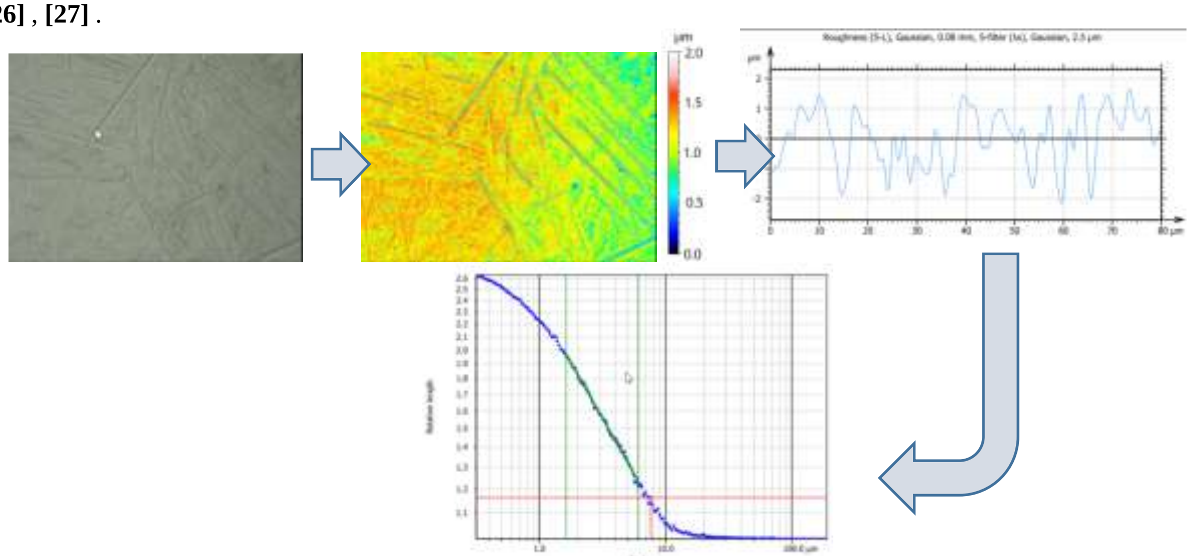

Figure 3:- Fractal Dimension Calculation and Analysis Started from SEM Image to Scale-Sensitive Fractal Analysis

To perform fractal dimension analysis using scanning electron microscopy (SEM) images, the following steps are typically involved (as shown in **Figure 3**):

1. Image Acquisition from SEM imaging provides detailed information about the material's surface topography and fine structures;
2. The acquired SEM image is preprocessed to improve the quality of the image and highlight the features of interest;
3. To analyze the fractal properties of specific structures within the SEM image, segmenting the image into distinct regions or objects is often necessary. This can be done using various image processing techniques such as thresholding, edge detection, or region-growing algorithms. In this work, the images were transformed into pseudo-color versions;
4. Fractal Dimension Calculation: The next step is to calculate their fractal dimension once the image or specific objects of interest are segmented. Several methods are available for this purpose, including box-counting, perimeter-area ratio, and Fourier analysis. These methods estimate the fractal dimension based on the scaling behavior of the object at different levels of magnification;
5. Box-counting: This method involves dividing the object into a grid of smaller boxes and counting the number of boxes that contain a portion of the object. The fractal dimension is determined by how the number of boxes changes with the size of the boxes;
6. Fractal dimension is obtained by analyzing the scaling relationship between the object's perimeter and its area;
7. The fractal dimension was derived from the power spectrum or fractal dimension spectrum of the transformed data;
8. Scale-Sensitive Fractal Analysis: Fractal analysis is scale-sensitive at multiple scales or resolutions aiming at the assessment of self-similarity or complexity across different levels of detail, revealing any scale-dependent fractal properties;
9. Interpretation and Applications: Once the fractal dimensions are calculated, they can be interpreted in the context of the specific system or material being studied.

Overall, fractal dimension calculation and analysis quantitatively measure the complexity and self-similarity of structures found in SEM images. This approach enables us to gain insights into the underlying patterns and characteristics of the objects under investigation.

The results of microstructure observations after the Ti-6Al-4V ELI sample was given heat treatment temperature of 850^{o}C, 950^{o}C, and 1050^{o}C shown in **Figure 4(a), 4(b),** and **4(c)**. As explained in **Figure 3**, SEM image was converted into a pseudo-color image and a 2D profile of surface roughness derived from the pseudo-color image; volume calculation, and surface Sk parameters observation; and calculation of surface's fractal dimension based on surface contour's fractal analysis.

At the 850^{o}C dissolution treatment temperature, as shown in **Figure 4(a)**, there was a significant change in microstructure, and the dendrite structure was no longer visible. The α phase is seen to form blocks or fragments similar to sharp (acicular) needles, such as martensite. The system developed is quite smooth and relatively uniform. This structure proves that the heat treatment process can improve the casting result's design and change the alloy's microstructure. The heat treatment process changes the phase composition, size, and phase distribution of α + β alloys **[28]** . Dissolution treatment followed by aging is usually performed to precipitate the α phase and produce a subtle mixture of α and β phases in the retained β or transformed β phases. At a dissolution treatment temperature of 950^{o}C, the α phase initially in partial flakes appears enlarged and rounded. These changes occur in some areas or parts of the alloy and are not yet thorough. Part of the phase of the α is still in the form of blocks or fragments, but it is starting to get rough. The microstructure looks inhomogeneous in shape and consists of a mixture of several morphological phases. Meanwhile, the microstructure looked homogenous at a temperature of 1050^{o}C, and the surface morphology shows α and β stages. The structure of these two phases is no longer sharp and pointed at both ends but more rounded.

The observations of surface properties after the heat treatment process show a close relationship between heat treatment temperature and fractal dimension. Heat treatment at a temperature of 850^{o}C produces a smoother surface than heat treatment at a temperature of 950^{o}C.

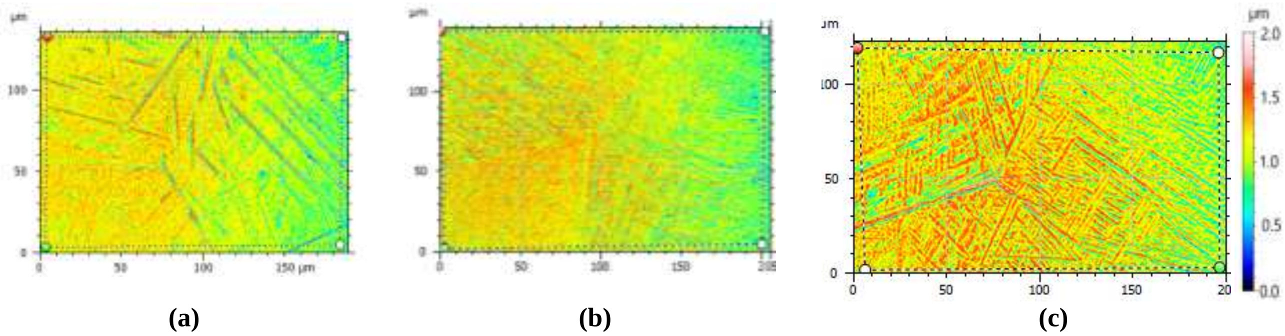

Figure 4:- Valley Depth After Undergoing a Heat Treatment of (a) 850°C, (b) 950°C, and 1050°C.

Table 1:- Valley Depth Measurment.

No.	Parameters	Original	Heat Treatment Temperatures			Unit
			850°C	**950°C**	**1050°C**	
1.	Horizontal area	24.443.02	23,119.00	26,805.00	22,376.00	μm^2
2.	Valley Area	201,657.91	93,958.00	152,269.00	105,550.00	μm^2
3.	Complexity	579.32	306.40	468.10	371.70	%
4.	Depth	18.66	12.59	13.07	15.23	µm
5.	Volume	28,565.00	11,003.00	16,002.00	14,917.00	μm^3
6.	Perimeter	722.90	616.80	667.20	616.50	µm

To determine the valley depth following various thermal treatments (as shown in **Table 1**), it is necessary to analyze a number of parameters, such as the calculated horizontal area, valley area, complexity, depth, volume, and perimeter. It provides precise values for these parameters with specific information about the material or the character of the heat treatment procedure, as listed in the table. It enables us to describe how each parameter relates to the heat treatment procedure and its potential impacts on valley depth. It needs to note that Calculated Horizontal Area is the entire horizontal surface area of the material being analyzed. The heat treatment procedure may alter the microstructure of the material, resulting in alterations to the horizontal area. Certain thermal treatments, such as annealing or recrystallization, can result in grain growth or phase transformations, which can impact the horizontal area calculation. Valley Area is the total area of the valleys or low points on the surface of the material. It is affected by surface roughness, texture, and the applied thermal treatment. Different thermal treatments can produce varying degrees of surface roughness, which can impact the valley area. Complexity refers to the intricacy and irregularity of the surface of the material. It is frequently evaluated with fractal analysis or other quantitative methods. Heat treatments can alter the microstructure and surface morphology of a material, potentially altering the surface complexity and canyons. Valley depth measures the vertical extent of the valleys on the surface of the material. It is directly proportional to the difference in elevation between summits and valleys. The heat treatment procedure can alter the topography of the material, resulting in variations in valley depth. Higher temperatures during thermal treatment can result in surface diffusion, grain growth, and phase transformations, which can affect the valley depth **[14]** ,**[16]** ,**[25]**

Table 1:- Sk and Volume Parameters for Analysis of Ti6Al4V ELI after undergoing Heat Treatment Temperature of 850°C, 950°C, and 1050°C.

Parameters – Extracted Channel											
	Sk Parameters - ISO 25178							**Volume Parameters - ISO 25178**			
Symbol	Original	850°C	950°C	1050°C	unit	Symbol	Original	850°C	950°C	1050°C	unit
S_k	6.90	4.79	6.17	6.02	µm	V_{mp}	0.092	0.084	0.084	0.089	$\mu m^3/\mu m^2$
S_{pk}	2.23	1.86	1.65	1.43	µm	V_{mc}	2.314	1.847	2.210	2.172	$\mu m^3/\mu m^2$
S_{vk}	3.04	2.73	2.34	2.48	µm	V_{vc}	2.885	2.087	2.835	2,608	$\mu m^3/\mu m^2$
S_{mrk1}	9.11	6.09	8.53	8.11	%	V_{vv}	0.555	0.270	0.262	0.258	$\mu m^3/\mu m^2$
S_{mrk2}	84.98	86.53	89.73	89.71	%						

The volume parameter (**Table 2**) represents the quantity of material within the region being analyzed. It is affected by the material's density and the surface's geometric characteristics. Heat treatments that result in material loss, such as sublimation or evaporation, can impact the volume of the material, potentially resulting in valley changes.

Perimeter is the total length of the boundary between the valleys and peaks on the surface of a material. It reveals the contour and irregularity of surface features. Surface morphology can be altered by heat treatments, thereby modifying the rim of valleys **[22]** .

Table 2:- Surface roughness parameters of the three different temperatures of Heat treatments.

ISO 4287 – Roughness (S-L)						
F: Leveled (LS), Angle 1.869^o; L-filter (λc): Gaussian. 0.08 µm						
S-filter (λs): Gaussian, 2.5 µm ; Evluation length: All λc (1):						
Amplitude parameters						
	Heat Treatment Temperature					
	850^{o}C	**950^{o}C**	**1050^{o}C**			Parameters' names
R_p	1.658	3.195	3.611	µm		The maximum peak height of the roughness profile
R_v	2.122	4.037	3.898	µm		The maximum valley depth of the roughness profile
R_z	3.780	7.232	7.509	µm		The maximum height of the roughness profile
R_t	3.780	7.232	7.509	µm		Total height of the roughness profile
R_a	0.7706	1.160	1,424	µm		Arithmetic means deviation of the roughness profile.
R_q	0.9267	1.453	1.736	µm		Root mean square (RMS) deviation of the roughness profile.
R_{sk}	-0.3608	-0.3451	-0.2343			The skewness of the roughness profile
R_{ku}	2.179	2,849	2.326			Kurtosis of the roughness profile
Spacing parameters						
R_{sm}	6.333	4.657	6.947	µm	No averaging (single value)	Mean width of the roughness profile elements
R_{dq}	43.82	63.56	-61.68	deg		The root-mean-square slope of the roughness profile
Material ratio parameters						
R_{mr}	29.29	5.277	6.596	%	C = 1 µm below the highest peak:	The relative material ratio of the roughness profile
R_{dc}	1.865	2.305	3.083	µm	p = 20%, q = 80%	Roughness profile section height difference
R_{mr} (R_z/4)	18.73	9.235	13.72	%	C = Rz/4 µm above mean plane	The automatic relative material ratio of the roughness profile

As shown in **Table 3**, the surface roughness parameters for the Ti6Al4V ELI alloy after heat treatments at different temperatures (850°C, 950°C, and 1050°C), parameters written provide insights into the surface roughness characteristics. These parameters are calculated based on the height deviations of the surface profile from a reference plane. As the roughness increased, the fractal dimension rose linearly **[29]** . The mechanism, which in turn depends on the microstructures or heat treatment conditions, is connected to the roughness of the surfaces. The measured surface roughness and fractal dimension values agreed with the observed surface topography **[22]** . It was reported by Venkatesh et al. that three-dimensional tests showed a correlation between the fractal dimension and the measured roughness of the heat-treated surfaces. As a result, the surface roughness brought on by various heat treatment conditions was principally responsible for the change in strength and ductility with fractal dimension **[29]** . In conclusion, the fractal dimension of the Ti-6Al-4V ELI alloy changes with the alteration of surface roughness under various heat treatment conditions.

As the roughness increased, the fractal dimension rose linearly **[29]** . The mechanism, which in turn depends on the microstructures or heat treatment conditions, is connected to the roughness of the surfaces. The measured surface roughness and fractal dimension values agreed with the observed surface topography **[22]** . It was reported by Venkatesh et al. that three-dimensional tests showed a correlation between the fractal dimension and the measured roughness of the heat-treated surfaces. As a result, the surface roughness brought on by various heat treatment conditions was principally responsible for the change in strength and ductility with fractal dimension **[29]** . In conclusion, the fractal dimension of the Ti-6Al-4V ELI alloy changes with the alteration of surface roughness under various heat treatment conditions.

Table 3:- Calculated Fractal Dimension for temperature heat treatment of 850^{o}C, 950^{o}C, and 1050^{o}C.

Heat Treatment Temperature	D_1	D_2	D_3
Original	2,932	2.774	2.899
850^o C	1.356	1.539	2.650
950^o C	2.788	2.803	2.814
1050^o C	1.267	1.388	1.494

The fractal dimension analysis results show that the fractal dimension is smaller than the fractal dimension heat treatment at 950^{o}C. Surface roughness after heat treatment temperature at 1050^{o}C is smoother than at 850^{o}C and 950^{o}C. This result confirms a study on the titanium alloy T16A14V surface roughness alteration due to the implementation of heat treatment **[30]** . A strong correlation between surface topography with Fractal Dimension was found in this research. This correlation confirms research work conducted by several authors **[14]** ,**[16]** ,**[25]** .

Conclusion:-

The predicted fractal dimensions produced by the current method for the three different heat-treating temperatures. The ingots carried out a heat treatment with solution treatment fast in a water medium (quenching). The treatment used variable temperatures, including 850^{o}C, 950^{o}C, and 1050^{o}C. The SEM images of the Ti-6Al-4V ELI sample were translated into topographic data The Fractal Dimension (FD) calculation results that the topography's microstructure appearing throughout the heat treatment temperatures and having fractal features. The results of microstructure observations after the Ti-6Al-4V ELI samples were given heat treatment temperature of 850^{o}C, there was a significant change in microstructure, and the dendrite structure was no longer visible.

The heat treatment improves the casting result's structure and changes the alloy's microstructure. The heat treatment process shows a close relationship between heat treatment temperature and fractal dimension. The fractal dimension analysis results show that the fractal dimension is smaller than that of the fractal dimension heat treatment at 950^{o}C.

Acknowledgments:-

With the completion of this article, allow us to express our gratitude and appreciation to our institution, namely the National Agency for Research and Innovation (BRIN), the Republic of Indonesia, which has provided the research funding and opportunity to prepare the article.

References:-

[1] ASTM-International. (2013). Standard Specification for Wrought Tutanium-6 Aluminum-4Vanadium ELI (Extra Low Interstitial) Alloy for Surgical Implant Applications (UNS R56401).

[2] Milovanović, A., Sedmak, A., Grbovic, A. S., & Čolić, K. (2020). Design Aspects of Hip Implant Made of Ti-6Al-4V Extra Low Interstitials Alloy. The 1st Mediterranean Conference on Fracture and Structural Integrity, MedFract1. 26, pp. 299-305. Athens, Greece: Procedia Structural Integrity . doi:10.1016/j.prostr.2020.06.038

[3] McAndrew, A. R., & Flipo, B. C. (2018). Linear Friction Welding for Near Net Shape Manufacturing of Titanium Alloy Ti-6Al-4V Aerospace Components. 2018 9th International Conference on Mechanical and Aerospace Engineering (ICMAE). doi:10.1109/ICMAE.2018.8467692

[4] Baltatu, M. S., Chiriac-Moruzzi, C., Vizureanu, P., Tóth, L., & Novák, J. (2022). Effect of Heat Treatment on Some Titanium Alloys Used as Biomaterials. Applied Sciences, 12(11241), 1-15. doi:10.3990/app122111241

[5] Suhendra, N., Setiawan, H., Purwati, H., & Lukmana. (2022). Analysis of Heat Treatment Results of Ti6Al7Nb for Application as Total Hip Arthroplasty Component Material. Journal of Research and Community Service, 3(9), 859-873.

[6] Zhong, C., Liu, J., Zhao, T., Schopphoven, T., Jinbao, Gasser, A., & Schleifenbaum, J. H. (2020). Laser Metal Deposition of Ti6Al4V - A Brief Review. Applied Science, 10(764), 1-12. doi: 10.3390/app10030764

[7] Sugahara, T., Reis, D. A., Neto, C. M., Neto, F. P., & Hirschmann, A. C. (2010). The Effect of Widmanstätten and Equiaxed Microstructures of Ti-6Al-4V on the Oxidation Rate and Creep Behavior. Materials Science Forum Vols, 657-662.

[8] Masinah, E., Greenwood, J. A., & Chetwynd, D. G. (2001). Metrology and Properties of Engineering Surfaces. doi:10.1007/978-1-4757-3369-3

[9] Kulesza, S., & Bramowicz, M. (2014). A comparative study of correlation methods for determination of fractal parameters in surface characterization. Applied Surface Science, 293(2014), 196-201.

[10] Yang, X., & Jin, T. (2021). Fractal calculation method of friction parameters: Surface morphology and load of galvanized sheet. Physics. doi:doi.org/10.1515/phys-2021-0042

[11] D. Risovića, Mahović, S., Poljaček, & M.Gojob. (2009). On correlation between fractal dimension and profilometric parameters in characterization of surface topographies. Applied Surface Science, 255(7), 4283-4288. doi:10.1016/j.apsusc.2008.11.028

[12] Lashgari, A., Ghamami, S., Shahbazkhany, S., Salgado-Morán, G., & Glossman-Mitnik, D. (2015). Fractal Dimension Calculation of a Manganese-Chromium Bimetallic Nanocomposite Using Image Processing. Journal of Nanomaterials, 2015, 1-9. Retrieved from HTTPS://DX.DOI.ORG/10.1155/2015/384835

[13] Pfeifer, P. (1984). Fractal Dimension as Working Tool for Surface-Roughness Problems. Application of Surface Science, 18(1984), 146-164.

[14] Ayala-Landeros, J. G., Castaño-Meneses, V. M., Becerra-Rodríguez, M. B., Servín-Guzmán, S., Román-Flores, S. E., & Olivares-Ramírez, u. M. (2018). Correlation between Roughness (Ra) and Fractal Dimension (D) Using Artificial Vision Systems for On-Site Inspection. Computación y Sistemas, 22(4), 1405-4446. doi:10.13053/cys-22-4-2785

[15] Truckenbrodt, R. J. (2004, January). A Simple Fractal Analysis Method of the Surface Roughness. Journal of Materials Processing Technology, 145(1), 40-45. doi:10.1016/S0924-0136(03)00860-4

[16] Hotar, V., & Salac, P. (2014, August 27). Surface Evaluation by Estimation of Fractal Dimension and Statistical Tools. The Scientific World Journal(Computer Intelligence in Modeling, Prediction, and Analysis of Complex Dynamical Systems), 1-11. doi:10.1155/2014/435935

[17] Movassagh, A., Haghighi, M., Zhang, X., Kasperczy, D., & Sayyafzadeh, M. (2021). A fractal approach for surface roughness analysis of laboratory hydraulic fracture. Journal of Natural Gas Science and Engineering, 85(January), 1-30. doi:10.1016/j.jngse.2020.103703

[18] Liang, X., Lin, B., Han, X., & Chen, S. (2012). Fractal analysis of engineering ceramics ground surface. Applied Surface Science, 258(17), 6406-6415. doi:10.1016/j.apsusc.2012.03.050

[19] Risovic, D., Gašparović, B., & B.Ćosović. (2003, August 21). Hydrodynamic influence on the fractal morphology of the linoleic acid adsorbed layer at the mercury/electrolyte interface. Colloids and Surfaces A: Physicochemical and Engineering Aspects, 223(1-3), 145-156. doi:10.1016/S0927-7757(03)00150-X

[20] Krim, J., Heyvaert, I., Haesendonck, C. V., & Bruynseraede, Y. (1993). Scanning Tunneling MicroscopyObservation of Selt-Affine Fractal Roughness in Ion-Bombarded Film Surfaces. Physical Review Letters, 7(1), 57-63.

[21] Shelberg, M. C., Lam, N. S., & Moellering, H. (1983). Measuring the Fractal Dimensions of Surfaces. Ohio: The Ohio State University.

[22] Kanygina, O. N., Chetverikova, A. G., Filyak, M. M., & Ogerchuk, A. A. (2016, 11 11). Fractal Approach to the Analysis of Ceramic Surfaces. Science for Ceramics Production in Glass and Ceramics, 72(11-12), 444-448. doi:10.1007/s10717-016-9807-x

[23] Damisih, D., Jujur, N., Bakri, A., & Prajitno, D. (2018). Pengaruh Temperatur Perlakuan Pelarutan terhadap Karakteristik Struktur Mikro dan Sifat Kekerasan Paduan Coran Ti-6Al-4V ELI. Widyariset, 4(2), 153-162. doi:10.14203/widyariset.4.2.2018.153-162

[24] Mojzes, I., Dominkovics, C., Harsányi, G., Nagy, S., Pipek, J., & Dobos, L. (2007). Heat treatment parameters effecting the fractal dimension of AuGe metalization on GaAs. Applied Physics Letters, 91, 1-3.

[25] Clarke, K. (1986). Computation of the Fractal Dimension of Topographic Surfaces Using the Triangular Prism Surface Area Method. Computers & Geosciences 12(5):713-722, 12(5713-722). doi:10.1016/0098-3004(86)90047-6

[26] Pinke, P., & Réger, M. (2005). Heat Treatment of The Casted Ti6Al4V Titanium Alloy. Materials Science and Technology,, 5(1), 1-6.
[27] KGaA. Oh, S. W. (2015). Effects of Heat Treatment on Mechanical Properties of VAR- Cast Ti-6Al-4V Alloy. In Proceeding of the World Congress on Mechanical, Chemical, and Material Properties of VAR Cast Ti-6Al-4V Alloy, (p. 1).
[28] Donachie, M. J. (2000). Titanium: A Technical Guide (2nd ed.). Ohio: ASM International.
[29] Venkatesh, B., Chen, D., & Bhole, S. D. (2008). Three-dimensional fractal analysis of fracture surfaces in a titanium alloy for biomedical applications. Scripta Materialia, 59(4), 391-394. doi:10.1016/j.scriptamat.2008.04.010
[30] Altug, M., Erdem, M., Ozay, C., & Bozkır, O. (2016). Surface roughness of Ti6AI4V after heat treatment evaluated by artificial neural networks. Materials Testing, 58(3), 189-199. doi: 10.3139/120.110844.